Broadband and tunable one-dimensional strongly nonlinear acoustic metamaterials: Theoretical study

Xin Fang,[*] Jihong Wen,[†] Jianfei Yin,[‡] Dianlong Yu, and Yong Xiao
Laboratory of Science and Technology on Integrated Logistics Support, National University of Defense Technology, Changsha 410073, Hunan, China

(Received 19 April 2016; revised manuscript received 4 August 2016; published 4 November 2016)

This paper focuses on the dispersion properties and mechanism of the one-dimensional strongly nonlinear acoustic metamaterials (NAMMs) based on the homotopy method. The local bifurcation mechanism, which is different from conventional local resonance, is found. It is demonstrated that the local period-doubling bifurcation of multiple cells will induce chaotic bands in the NAMMs, which can significantly expand the bandwidth for wave suppression. The saddle-node bifurcation leads the system state jumping to the chaotic branch. Furthermore, the amplitude-dependent dispersion properties enable NAMMs to manipulate elastic waves externally. Study of broadband tunable abilities reveals that stronger nonlinearity (larger nonlinear coefficient or higher amplitude) presents a broader nonlinear band gap and larger transmission loss. Moreover, with less attached mass, a low frequency and broadband are achievable simultaneously. This research may provide useful approaches for elastic wave control.

DOI: 10.1103/PhysRevE.94.052206

I. INTRODUCTION

Acoustic metamaterials (AMMs) are typically artificial periodic media structured on a size scale smaller than the wavelength of external stimuli [1–3]. There has been a great deal of interest in designing AMMs to exhibit interesting and extraordinary negative indices [3–9]. Numerous studies [3–11] focus on linear AMMs (LAMMs) based on the locally resonant mechanism first found by Liu *et al.* [2]. The locally resonant band gaps in LAMMs are widely used for wave manipulation [1,12,13]. However, the band gaps and wave propagation in LAMMs are manipulated mainly through material and structural parameters.

The presence of nonlinear interaction can enhance the responses of periodic structures [1] and can be used for acoustic elements [14,15]. Nonlinear periodic structures (NPSs) [16–18] exhibit special band-gap properties, such as amplitude dependence [19], wave coupling [20], subharmonic frequency [21,22], discrete breathers [23], solitons [24,25], and Rayleigh-type surface waves [26]. Therefore, NPSs and nonlinear AMMs (NAMMs) have been attracting increasing attention. Previous investigations have mainly focused on discrete chains and granular crystals [19] interacting nonlinearly through Hertzian contact [27] building upon Nesterenko's works [28]. Simulations and experiments demonstrate that there are bifurcations and highly nonlinear traveling waves in granular crystals [17,18,29]. Amplitude-dependent dispersion properties [30] and wave beaming [31] in periodic granular media have been observed. Acoustic switching, rectification devices, and logic elements have been realized based on the bifurcations [17] and band-gap effects [18]. Subsequently, wave propagation in layered NPSs was considered and second-harmonic waves were observed [32]. Furthermore, the critical amplitude for energy transmission [33] and bifurcation-induced band-gap reconfiguration [34] in one-dimensional (1D) NPSs have been studied experimentally. Herbold *et al.* [35] studied the wave propagation in a diatomic granular crystal chain and found that the band-gap effect has a significant influence on signal transformation; they proved that its limited frequencies of the acoustic band gap can be tuned by varying the particle's material properties, mass, and initial compression. A 1D strong NAMM has been proved to increase the sound speed and acoustic impedance [36]. A nonlinear acoustic lens with a tunable focus was achieved with granular crystals [37]. Midtvedt *et al.* [38] designed nonlinear phononics using atomically thin membranes and studied their localized flexural modes. The works mentioned above reveal that the dispersion properties, mechanisms, and physical effects of strong NAMMs are interesting but have not been fully studied.

This paper considers a basic 1D model of a NAMM. In Sec. II we describe our model; the numerical method for vibration responses is introduced, and nonlinear modes and chaotic responses of simplified cells are studied. Our main results are presented in Secs. III and IV. In Sec. III we find that there is a chaotic band in NAMM, which significantly expands the bandwidth for wave suppression; the mechanism analysis demonstrates that the chaotic band is induced by the local bifurcations of multiple cells and the bifurcation-induced state transitions are revealed. Subsequently, the methods to manipulate the nonlinear band gaps with a chaotic band are presented in Sec. IV. The homotopy approach adopted to calculate the dispersion curves is elaborated in the Appendix.

II. MODEL AND BASIC DYNAMICS

A. The 1D model of nonlinear acoustic metamaterial

In the 1D basic model of a NAMM, the nonlinear oscillators with cubic stiffness ($f_{\mathrm{nl}} = k_1 x + k_2 x^3$) are attached to the 1D linear chain, as shown in Fig. 1. This model can explain the important dynamics of the NAMM.

[*]Corresponding author: xinfangdr@sina.com
[†]Corresponding author: wenjihong@vip.sina.com
[‡]Corresponding author: nmhsyjf@hotmail.com

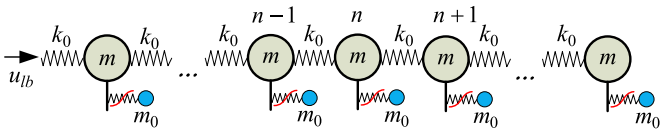

FIG. 1. Basic model of a 1D NAMM.

Defining u and y as displacements of the linear and nonlinear oscillators in each cell, respectively, with the Bloch theorem $u_{n+1} = u_n \exp(-i\kappa a)$ of the periodic structures, the generalized motion function of the system is transformed into

$$\omega^2 u''(\tau) + \alpha^2 u(\tau) = \lambda\beta_1(y-u) + \lambda\beta_2(y-u)^3,$$
$$\omega^2 y''(\tau) = -\beta_1(y-u) - \beta_2(y-u)^3. \quad (1)$$

The definitions of the parameters are as follows: $\tau = \omega t$, $\omega_s = \sqrt{k_0/m}$, $\lambda = m_0/m$, $\beta_1 = k_1/m_0$, $\beta_2 = k_2/m_0$, $p = \kappa\alpha$, κ is a wave vector, α symbolizes the lattice constant $\alpha = \omega_s\sqrt{2(1-\cos p)}$, and the generalized frequency is $\Omega = \omega/\omega_s$. The prime denotes the differentiation with respect to the variable τ.

The numerical integral approach is also adopted to explore the response properties of the nonlinear system. The excitation displacement $u_{lb}(t) = A_0 \sin\omega t$. In the simulations, the mass $m = 1$. The natural frequency of the primary structure is $\omega_s = \sqrt{10\pi}$. The total nonlinear stiffness of the attached nonlinear oscillator is the first differential of the nonlinear restoring force, that is, $\beta_1 + 3\beta_2\Delta^2$. We objectively assess the strength of nonlinearity by comparing the linear stiffness β_1 with the nonlinear stiffness $3\beta_2 A_0^2$. Defining the strength factor of nonlinearity as $\sigma = 3\beta_2 A_0^2/\beta_1$, if $\sigma \ll 1$, it is a weak nonlinearity; if $0.1 < \sigma < 0.3$, it is a moderate nonlinearity; and if $\sigma > 0.3$, it is a strongly nonlinear system. In the simulations below, the five cases with different β_2 are employed to represent different nonlinear strengths. The parameters are $\lambda = 0.5$, $\beta_1 = 15\pi$, $A_0 = 0.005$; L1, $\beta_2 = 0$; N1, $\beta_2 = 2\times10^4$($\sigma = 0.032$, weakly nonlinear); N2, $\beta_2 = 1\times10^5$($\sigma = 0.16$, moderately nonlinear); N3, $\beta_2 = 2\times10^5$($\sigma = 0.32$, strongly nonlinear), N4, $\beta_2 = 1\times10^6$($\sigma = 1.6$, strongly nonlinear). Here L denotes linear and N nonlinear.

B. Nonlinear dynamics of simplified cells

The basic characteristics of the NAMMs can be described with the help of a simplified model of a single cell, which is simplified as a two degree of freedom (2DOF) nonlinear system, as shown in Fig. 2(a). To be consistent with the responses of NAMMs, the excitation displacement applied to the linear oscillator of the simplified model is $u_{lb}(t)$.

With the harmonic balance method in Eq. (2), we can solve the steady amplitudes $\mathbf{X} = [A \quad B]^T$ of the simplified model

$$[\mathbf{K} - \omega^2\mathbf{M}]\mathbf{X} + \frac{3}{4}\boldsymbol{\beta}_{\rm nl}(A-B)^3 = \mathbf{F}_a,$$
$$\boldsymbol{\beta}_{\rm nl} = \begin{bmatrix}\lambda\beta_2\\ -\beta_2\end{bmatrix}, \quad \mathbf{F}_a = \begin{bmatrix}\omega_0^2 A_0\\ 0\end{bmatrix}, \quad (2)$$
$$\mathbf{M} = \begin{bmatrix}1 & 0\\ 0 & 1\end{bmatrix}, \quad \mathbf{K} = \begin{bmatrix}(\omega_0^2 + \lambda\beta_1) & -\lambda\beta_1\\ -\beta_1 & \beta_1\end{bmatrix}.$$

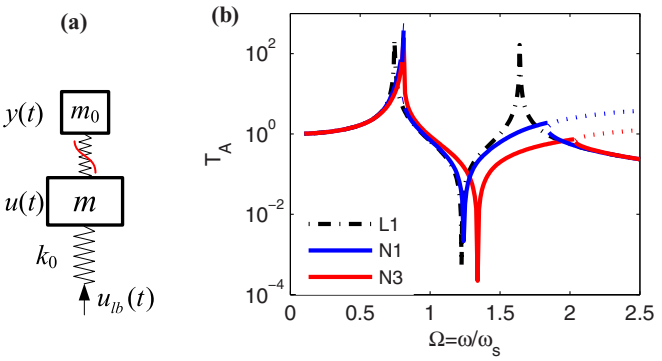

FIG. 2. (a) Simplified model of a single cell. (b) Frequency responses of the simplified model. The dotted section of the lines of N1 and N3 are unstable multiple solutions. Here the displacement transmissibility is defined as $T_A = A(B)/A_0$.

The solutions in the real domain express the fundamental nonlinear dynamic properties of the simplified model, as illustrated in Fig. 2(b).

The linear 2DOF system has two resonant modes corresponding to two linear modes (LMs). An LM is also a periodic trajectory. The nonlinearity has relatively less influence on the first LM, as shown in Fig. 2(b) [see also Figs. 4(a) and 4(c)]. However, the nonlinearity makes the second resonant LM disappear instead with nonlinear modes (NMs), which result in a broad range of weak response in Fig. 2(b). A nonlinear mode is defined as a two- dimensional invariant manifold in phase space [39–41]. As illustrated in Fig. 3, the invariant manifold of a linear mode is a straight line whose slope is $1/[1-(\omega/\omega_a)^2]$, with $\omega_a = \sqrt{\beta_1}$. In contrast, the invariant manifolds of the two NMs are curves [42]. The quasiperiodic long-term motion of the first NM forms a flexural region near the curve. However, the chaotic motion of the second NM in a long time interval forms a region containing disordered curves. For the system without damping, the lengths of the straight lines are infinite, but the volumes of the invariant manifolds of the two NMs are finite, which means that the motions are bounded. Therefore,

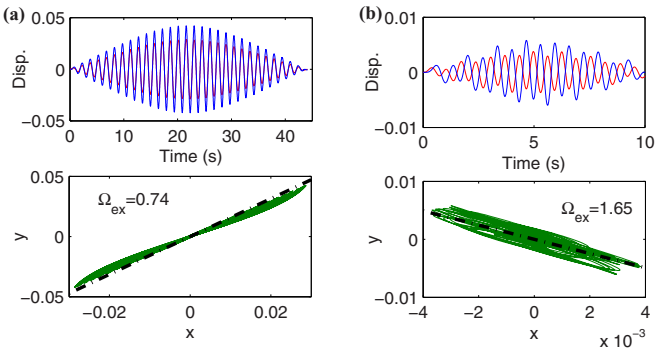

FIG. 3. Displacements (top graph) and invariant manifolds (bottom graph) of the simplified model in N3. In displacement plots, the red and blue lines represents $u(t)$ and $y(t)$, respectively. (a) First normal mode $\Omega = 0.74$ and in-phase motion. (b) Second normal mode $\Omega = 1.65$ and out-of-phase motion. The dash-dotted straight line and green curve represent the LM and NM, respectively. The slope of the straight line is $1/[1-(\omega/\omega_a)^2]$, where $\omega_a = \sqrt{\beta_1}$. In this case, $\Omega = 0.74$ is quasiperiodic but $\Omega = 1.65$ is chaotic.

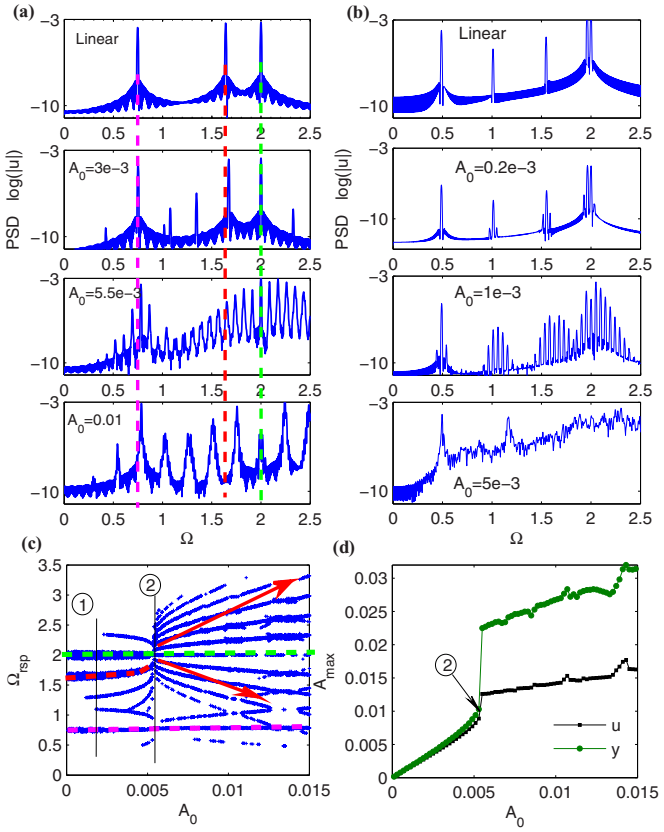

FIG. 4. Responses of the simplified single cell and NAMMs with different cell numbers under different excitation amplitude A_0 with a constant frequency $\Omega_{ex} = 2$ (and $\lambda = 0.5$, $\beta_1 = 15\pi$, and $\beta_2 = 10 \times 10^4$). (a) Numerically calculated power spectra of the simplified cell. (b) Numerically calculated power spectra of the nonlinear chain with two cells. (c) Main frequency components of the displacement $u(t)$ in the simplified cell. In (a) and (c), magenta, red, and green dashed lines correspond to the first LM, the second LM, and $\Omega_{ex} = 2$, respectively; the circled numbers 1 and 2 are bifurcation points. (d) Maximum displacement amplitude $u(t)$ of the single-cell change with excitation amplitude A_0.

the nonlinear modes have capacities to suppress the resonances in the linear regime.

This capacity to suppress resonance results from the nonlinear mode bifurcations and period-doubling bifurcations. Furthermore, these bifurcations may cause chaotic responses in the systems. The power spectra of a single cell and two cells indicate this procedure.

As shown in Figs. 4(a) and 4(b), both the power spectra of the simplified cell and the chain with two cells generate bifurcations under different ranges of driving amplitudes. Under the excitations $\Omega_{ex} = 2$ (this frequency is chosen in the optical branch in metamaterial below), the simplified cell generates bifurcations of the periodic solutions near the LMs and Ω_{ex}. The main frequency components in the displacement responses of the single cell are identified with a numerical method and are illustrated in Fig. 4(c). At point 1, period-doubling bifurcations appear in the neighborhood of the second LM [40] and Ω_{ex}, which causes the motions to degrade from periodic into quasiperiodic trajectories; in the interval between 1 and 2, the branch of the second LM merges with the excitation branch. After critical point 2, much more period-doubling bifurcations appear, so the motions cascade into chaos in the simplified cell. Point 2 is a saddle-node bifurcation point where a jump occurs. Further increasing the parameters will merge the frequency peaks; meanwhile, the peaks become sparser and move bilaterally but mainly upward. The power spectra of the chain with two cells also show this cascades route to chaos: Period bifurcations are stimulated near the four LMs but mainly near the two higher ones; when A_0 reaches a certain value, the motions will cascade into chaos. Furthermore, much lower amplitudes are needed for the two cells to cause chaotic motions than that of a single cell, because the chain with two chains has larger complexities (four degrees of freedom). Similarly, in the multicell chain model, even with a small A_0, much denser bifurcations will be produced near the multiple LMs and then chaos is generated.

The discussion above has expounded the frequency responses, the nonlinear modes, bifurcations, and the chaos induced by them in a simplified single cell and two-cell chains. In the following we discuss how these properties influence the band gaps and responses of the nonlinear acoustic metamaterial.

III. DISPERSION AND MECHANISM

A. Dispersion and response properties of the 1D metamaterial chain

The homotopy analysis method (HAM) [43], which is compatible with strongly nonlinear systems, is adopted in this paper to calculate the dispersion curves of a nonlinear periodic structure. The detailed HAM is elaborated in the Appendix.

To validate the analytical solutions and investigate the general characteristics of NAMMs, we use the directly numerical integration method on the finite periodic structures with 26 cells. Furthermore, a displacement boundary is applied to the left-end linear oscillator of the primary chain: The motion equation of the first oscillator is $m\ddot{u}_1 = k_0(u_2 + u_{lb} - 2u_1) + f_{NL}$. The excitation amplitude A_0 is also the amplitude of the initial guessed solution $u_0(t)$ of $u(t)$ in the HAM. The boundaries of the right-end linear oscillator are free and its steady responses are analyzed. The vibration transmissibility is defined as $T_A = A_{\max}/A_0$, where $A_{\max}$ is the maximum amplitude of the response displacement of the last linear oscillator from the actuator. For the systems with damping, a linear damping $m_0\mu(\dot{y} - \dot{u})$ is added in the nonlinear oscillators. Only weak damping is considered because the strong damping will suppress the nonlinear effect.

The influence of the nonlinearity degrees on band gaps and responses is investigated Figs. 5 and 6. The dispersion curves have two branches: acoustic and optical branches. These comparative studies indicate that both LAMMs and NAMMs have elastic wave band gaps, but there are essential distinctions of the band-gap structures between them: The HAM accurately predicts the boundaries of band gaps and dispersion curves of both weak and strong NAMMs, but the upper boundaries of band gaps of NAMMs become blurred in both T_A and power spectral density (PSD).

For finite LAMMs, the locally resonant mechanism generates a complete stop band near the natural frequency of

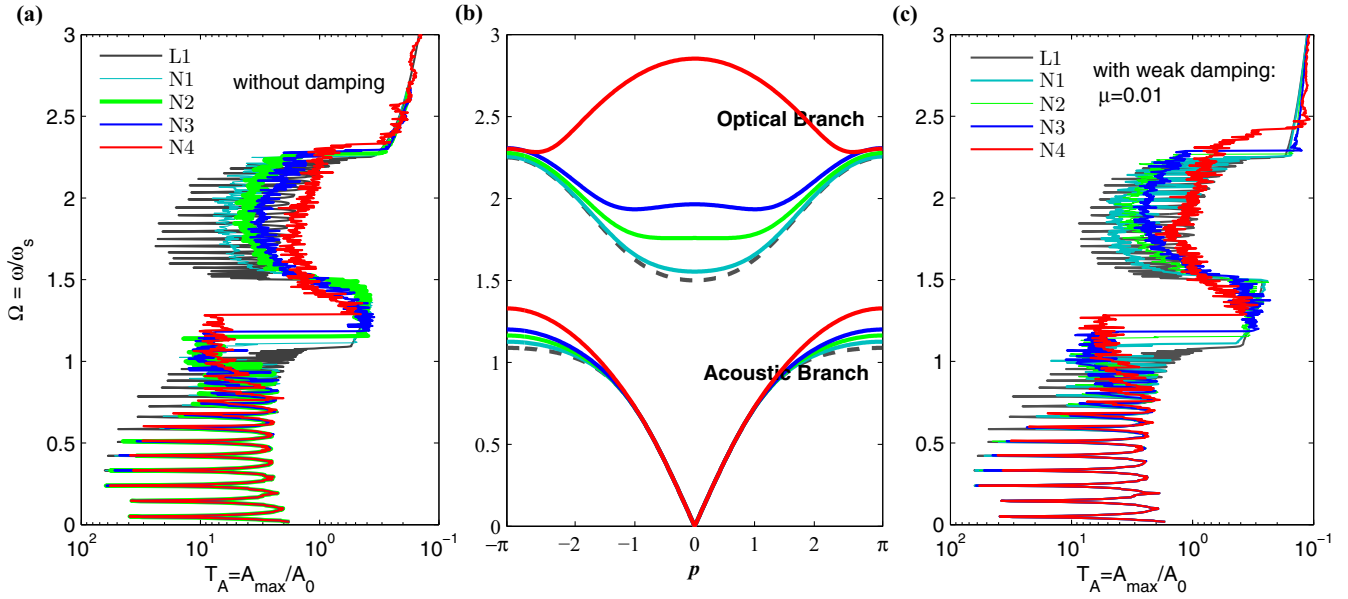

FIG. 5. (a) and (c) Frequency responses and (b) dispersion curves of LAMMs and NAMMs. The simulation time is 400 s. (a) Chain without damping. (c) Chain with weak damping $\mu = 0.01$; in this case, we find the maximum amplitude in the steady response interval 220–400 s. Different color curves in (b) correspond to the legends in (a) and (c).

the attached linear resonator [4,8] where the plane wave is attenuated. By contrast, the wave propagation occurs without attenuation in the passband, in which the LAMMs will generate multimode resonances. Unfortunately, the attached local resonators double the modal numbers of a finite structure, so the number of the resonances in the passband increases simultaneously. Increasing the cell number will also increase the resonances. These results indicate that LAMMs will generate violent responses in the passband, although the disturbances are attenuated in the band gap under nonmode excitation. Moreover, 1:1 resonances and the dense modes near this frequency are always prominent, so the wave energy is localized in a narrow band.

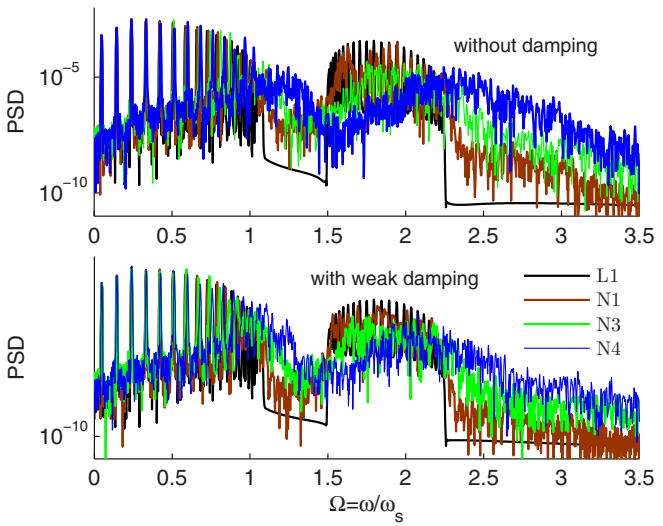

FIG. 6. Power spectral densities from the sine-sweep excitations. The sweeping frequency increases slowly from 0.1 to 10 Hz in 400 s.

The band-gap structures of the NAMMs are complex. In the range of the acoustic branch, the frequency responses (the maximum displacements) of NAMMs are similar to the corresponding linear ones, where the near-linear mode resonances still exist and vibration energy can be transmitted with a little attenuation. The simplified cells are helpful to explain this phenomenon: The responses of NAMMs in acoustic branches mainly depend on the low-frequency modes of multiple cells, but the nonlinearity mainly affects the high-frequency modes, therefore, they are similar to the LAMMs in this domain. However, there is an important difference. As shown in Fig. 3, the nonlinear modes have finite phase volumes, which mean that the amplitudes of NMs in acoustic branch are bounded even for the system without damping. The property also benefits low-frequency wave suppression.

For a weak NAMM with a low amplitude, its complete stop band is similar to that of the LAMMs. However, in the optical branch, the dense modal resonances are significantly suppressed, which causes the T_A of NAMMs to be much smaller than that of LAMMs. This effect on the optical branch (OB) is due to the hardening characteristic of the cubic spring. The frequency range is defined as the OB band. Furthermore, as the dispersion curves show, increasing the strength of nonlinearity will broaden the band gaps (without an OB band) while the T_A in the band gaps and OB bands decrease markedly. Power spectral densities from sine-sweep excitations in Fig. 6 also prove this result. Therefore, the width of the band gap reflects the wave transmissibility.

For the N4 case, the nonlinearity is strong enough and the maximum steady amplitudes are even lower than the minimum values of LAMMs. Its optical branch is approached by the HAM algorithm with convergence-control parameters $h_1 = 1$ and $h_2 = -7$. Because many frequency components are generated above $\Omega = 2.3$, as shown in Figs. 5 and 6, the frequency range of the optical branch of such a strong

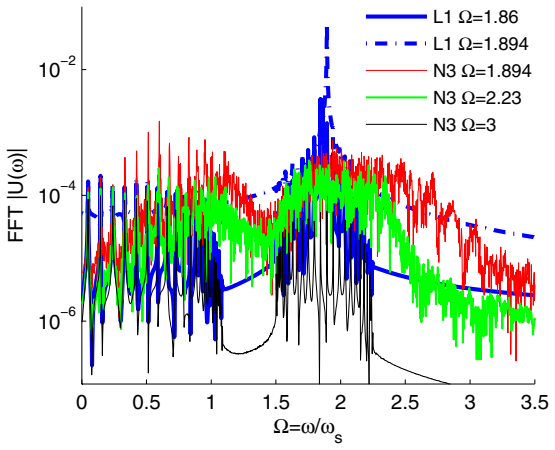

FIG. 7. Frequency spectra of the responses of LAMMs and NAMMs under different monofrequency excitations. The frequency spectra were obtained by a fast Fourier transform (FFT).

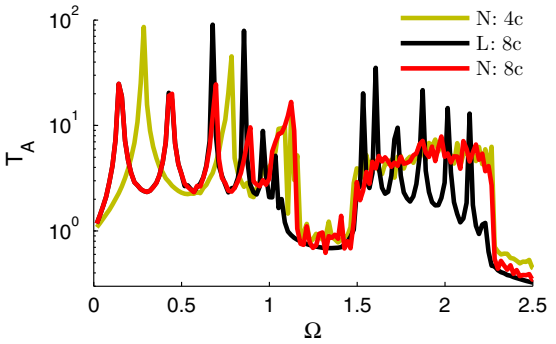

FIG. 8. Frequency responses of LAMMs and NAMMs with four and eight cells. Here nc represents that there are n cells in the chain. The parameters come from the N2 case.

NAMM exceeds $\Omega = 2.3$. This case indicates that OB band in the NAMM must be taken into consideration rather than considering band gap effect only, especially for the strongly nonlinear ones. Moreover, the interacting modes and the subharmonic (or superharmonic) resonances in NAMMs may be generated in the band gap; therefore, some of the energy can transfer into the band gap such that the nonlinear band gap may not be the complete stop band.

The influence of weak damping on dispersion properties is also studied. Both T_A and PSD indicate that although the weak damping partly attenuates the resonances in pass bands and weaken the high-frequency components, it will not change the essential properties stated above, because a weak damping will not stop the system from cascading into chaos for strong nonlinearity.

B. Mechanism: Bifurcation-induced chaotic band

To explore the mechanism of the OB bands of NAMMs significantly suppressing the wave propagations, the monofrequency responses of the metamaterials are presented. In Fig. 7 three excitation frequencies $\Omega = 1.894$, 2.23, and 3 are in the nonlinear band gap, the OB band, and the high-frequency stop band of N3, respectively. In addition, $\Omega = 1.894$ is exactly a resonant frequency. As is known, the wave energy in LAMMs is localized in 1:1 resonance or modal resonance frequencies. In contrast, for NAMMs, the frequency spectra indicate that a monofrequency excitation will generate a broadband response and exhibits band-gap behaviors. Therefore, the energy is redistributed to the broadband spectra but not localized at the 1:1 resonance or modal resonance frequencies as with LAMMs, which is an energy dispersion phenomenon. Further analysis of the spectra indicates that the strong nonlinearity induces chaotic responses, which formulate a chaotic band in Figs. 5(a) and 5(c). The chaotic band connects the nonlinear band gap and the high-frequency stop band. Furthermore, a low-frequency excitation can generate a broadband high-frequency response that exceeds the cutoff frequency of the passband, which is superharmonic and with mode interaction. We found that this is another mechanism in metamaterials that is different from the conventional local resonance and this mechanism in NAMMs enables both the band gap and chaotic band to suppress the wave propagations, which significantly expands the bandwidth for wave attenuation. Moreover, under the excitation in the high-frequency stop band, the response of NAMMs is similar to that of LAMMs, which is similar to the case under small amplitudes.

The dynamics of nonlinear cells shows the process cascading into chaos. For the simplified single cell, bifurcations are generated near the two LMs (mainly near the higher one) and the excitation frequency Ω_{ex} and it is easier to generate bifurcations of periodic trajectories near the four LMs of a two-cell chain and Ω_{ex}. However, in the multi-DOF NAMM model, much denser bifurcations are produced near the multiple LMs in the OB band, so we cannot identify the huge number of bifurcations: Then chaos is generated.

To better reveal the state transitions of the NAMM with multiple cells, we studied their bifurcation properties. To generate a stable stop band and a chaotic band that suppresses the resonances, only four cells are needed, as illustrated in Fig. 8. Further increasing the cell number hardly changes the response properties in the chaotic band.

To understand the transition between chaotic and periodic states occurring in the NAMM, we conduct parametric continuation using the Newton-Raphson (NR) [44] method on a NAMM chain with four cells under two driving frequencies $\Omega_{ex} = 2$ and 2.2. The responses from numerical integration of the motion equation of NAMMs with different numbers of cells are calculated. The results are illustrated in Figs. 9(a)–9(d). The damping effect is not considered here. Applying the Newton-Raphson method, we solve the family of periodic orbits as a function of driving amplitude A_0. The linear stabilities of periodic solutions are judged by Floquet multipliers of the Poincaré map of the state motion equations of the nonautonomous system [45]. When all multipliers are in the unit circle, the considered periodic solution is stable. When the multipliers leave the unit circle, bifurcation occurs. Each saddle-node (SN) bifurcation is responsible for changing the stability of periodic solutions. As a result of period-doubling bifurcation, the period of the solution is doubled.

In Figs. 9(a) and 9(b) the two frequencies present two typical bifurcation diagrams of the NAMM model. The

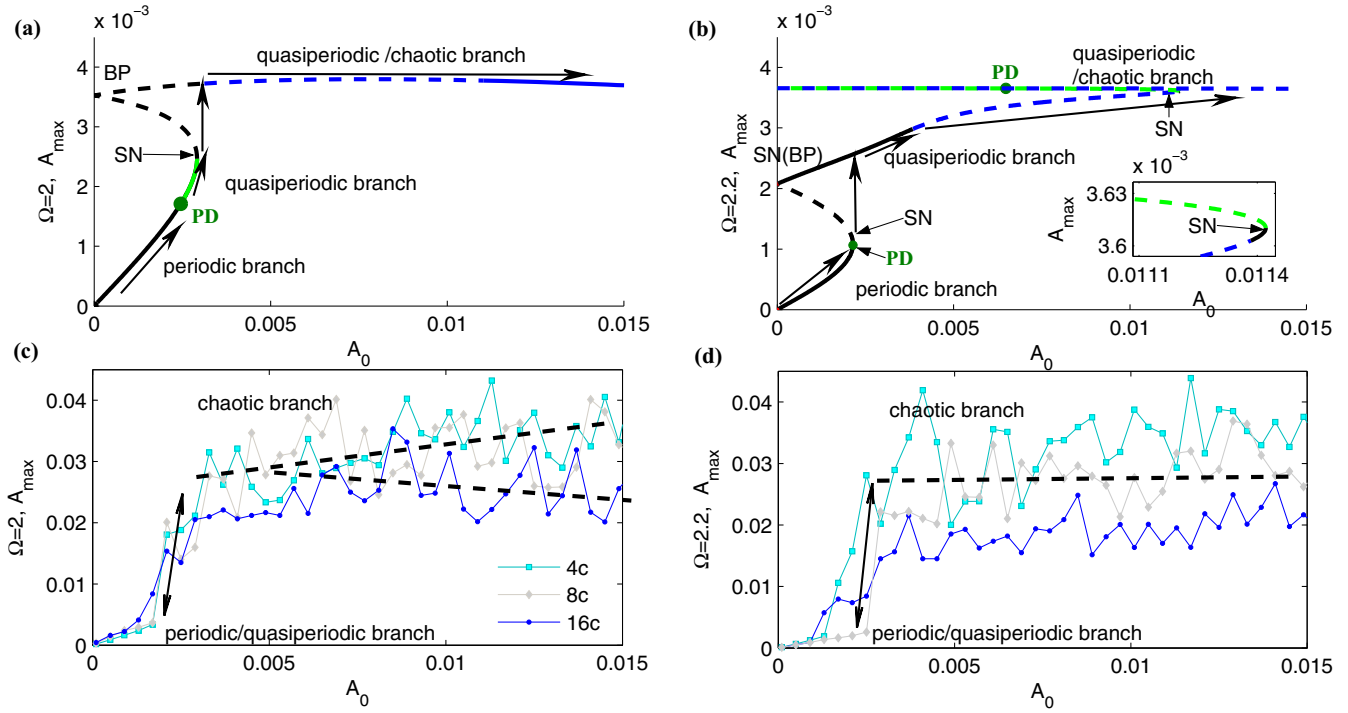

FIG. 9. Bifurcation, stability, and responses. The maximum displacement $A_{\max}$ as a function of driving amplitude A_0 under two driving frequencies ($\Omega_{ex} = 2$ and 2.2). (a) and (b) Numerical calculated bifurcation diagrams of the NAMM chain with four cells. The solid (dashed) lines correspond to the stable (unstable) branches. The properties of the different branches are labeled on the diagrams. The abbreviations are bifurcation points: SN, BP, and PD denote saddle-node bifurcation, branch point, and period-doubling bifurcation, respectively. Black arrows correspond to the path (and jump) followed with increasing driving amplitude. The PD bifurcation points are marked with green circles on the branches. (c) and (d) Maximum response displacements of NAMMs with different numbers of cells change with excitation amplitude A_0. The results are from the numerical integration. In the legend of (c) nc represents that there are n cells in the chain. Black dashed lines correspond to the average amplitudes. The integral time is 400 s. The system parameters are identical to the case N2.

maximum displacement responses (in 400 s) of NAMMs with different numbers of cells changing with excitation amplitude A_0 are shown in Figs. 9(c) and 9(d). We should mention that the integral time will influence $A_{\max}$ but will not change the state transitions.

Let us first take Fig. 9(a) as example. There is a stable periodic branch in the interval $0 < A_0 < 2.92 \times 10^{-3}$. A period-doubling (PD) bifurcation point appears at $A_0 = 2.45 \times 10^{-3}$. Generally, a PD bifurcation will start another branch. However, all the period-doubling branches of the NAMM are almost identical to the original monoperiodic branches and their linear stabilities are identical too, which means that all the branches above the PD bifurcation points become quasiperiodic obits. Before the PD bifurcation, the NAMM behaves as a LAMM, as shown in Fig. 9(c). At the first SN bifurcation point $A_0 = 2.92 \times 10^{-3}$, the stability transition makes the system jump to another branch. The jump point in Fig. 9(c) fits the SN bifurcation well. However, no stable periodic or quasiperiodic solutions are found with the numerical NR and Floquet methods in the following branch. Figure 9(c) illustrates that the NAMMs with 4, 8, and 16 cells jump to the chaotic branch. Although the periodic solutions in the interval $0.011 < A_0 < 0.015$ are stable, the responses still are chaotic. The averaged variation trends of the response curves are in accord with the blue quasiperiodic branch in the bifurcation diagram: $A_{\max}$ increases slowly and even decreases with A_0. Therefore, we can deduce that it is the chaotic response of the complex system that causes the nonexistence of stable periodic family solutions.

The bifurcation diagram under $\Omega_{ex} = 2.2$ in Fig. 9(b) has more complex structures but the laws are similar. The first PD bifurcation appears at $A_0 = 2.15 \times 10^{-3}$ near the first SN bifurcation. However, the state jumps to another stable quasiperiodic branch then. Similarly, the responses in this branch still are chaotic. Along the branch, except for a small interval near the second SN bifurcation point (in the magnified plot), no stable periodic family solutions are found because of chaos. The responses in Fig. 9(d) are consistent with the laws in Fig. 9(b).

The analysis above demonstrates that the period-doubling bifurcation causes the chaos and the SN bifurcation point makes the state jump to chaotic branches. In brief, the chaotic band in NAMMs (as a whole) is induced by the period-doubling bifurcations of multiple cells (in parts). We define this mechanism as a local bifurcation. Analyses of nonlinear modes of simplified cells indicate that the strong nonlinearity can suppress the resonant responses in quasiperiodic and chaotic regimes, so NAMMs can suppress the resonant modes (in LAMMs) in the OB bands.

IV. MANIPULATING BAND GAPS WITH A CHAOTIC BAND

The different properties of NAMMs are casued by the nonlinear stiffness $3\beta_2\Delta^2$ of the attached oscillators. Both

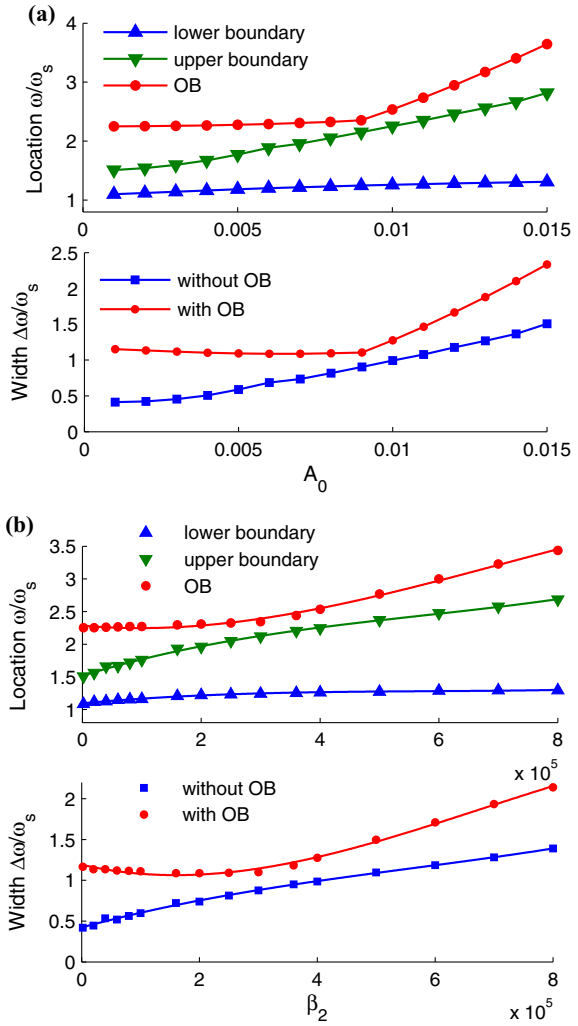

FIG. 10. Influences of nonlinear coefficients and amplitudes on band gaps of NAMMs (with $\lambda = 0.5$ and $\beta_1 = 15\pi$): (a) $\beta_2 = 1\times10^5$ and (b) $A_0 = 0.005$.

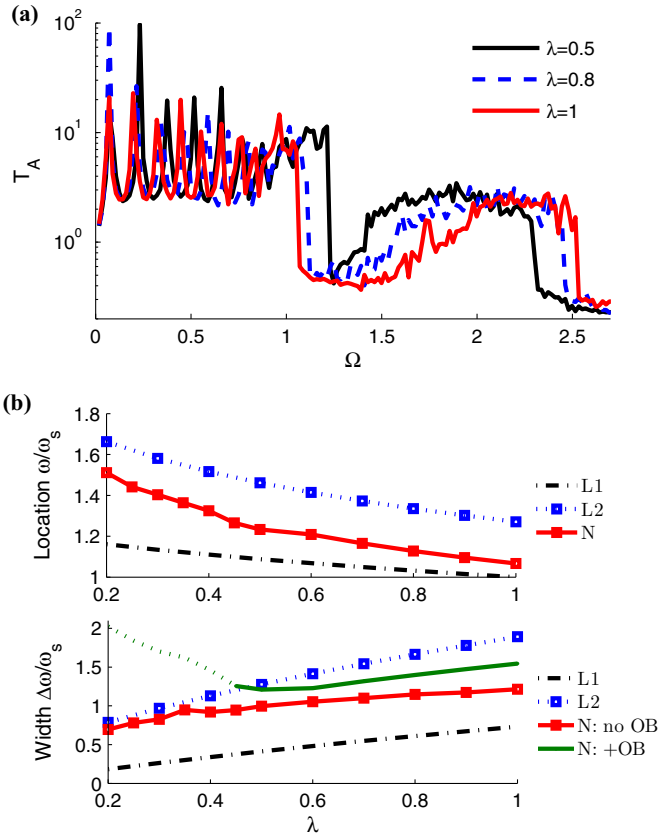

FIG. 11. Influences of mass ratio on (a) the frequency responses of NAMMs with 16 cells and (b) the band gaps. For L2, $\beta_1 = 50\pi$; for N, $\beta_1 = 15\pi$, $\beta_2 = 10\times10^4$, and $A_0 = 0.01$. Here no (+) OB denotes without(with) OB band.

A_0 and β_2 influence the nonlinear stiffness $3\beta_2\Delta^2$, therefore the band properties changing with β_2 and A_0 are similar, as illustrated in Figs. 10(a) and 10(b).

The energy-frequency dependence of the bifurcations causes the amplitude-frequency dependence of the band gaps of NAMMs. With increasing A_0, the lower boundary of the nonlinear band gap moves slowly, while its upper boundary shifts much faster to the high frequency; the upper boundary of the OB band remians almost constant for weak and moderate nonlinearities, but will increase when strong nonlinearity occurs. Therefore, the widths of the nonlinear band gap and total band increase. Higher amplitude gives rise to larger transmission loss, because higher amplitudes have more remarkable nonlinear effects. Therefore, the local bifurcation enhances the capacity and broadens the band to suppress elastic waves. Therefore, the amplitude dependence enables NAMMs to manipulate the elastic plane-wave propagations and this advantage is more prominent for strong NAMMs.

The nonlinear stiffness coefficient β_2 can also induce bifurcations to modulate the chaotic band. Combining the properties in Fig. 2, it is known that a larger β_2 causes lower responses and a smaller T_A when the chaotic band is formulated. Increasing β_2 can also broaden the nonlinear band gap (and the total band with the OB band will increase fast for strongly nonlinear NAMMs), while the lower boundary remains almost steady.

The mass ratio λ attached to the matrix attracts extensive attention in practice. As shown in Fig. 11, for both LAMMs and NAMMs, the lower boundaries of the band gaps shift downward with increasing λ. Although the band gaps' widths of LAMMs are expanded by increasing β_1, the expense is the elevation of their locations. Therefore, a broader band gap with less attached mass, and a low frequency and broadband for LAMMs may be contradictory [20]. By contrast, when $\lambda>0.5$, the dispersion characteristics of NAMMs enable them to achieve low frequency and broadband band gaps simultaneously. For the strong NAMMs with a low λ, the widths with an OB band may vary in a nonmonotonic way. That is because when $\lambda\to0$, the connections between the nonlinear oscillators and the primary masses approach rigidity, which make the structure tend to be a monatomic chain, whose normalized cutoff frequency of the pass band is $\Omega_c = 2$. Furthermore, as shown in Fig. 11(a), the average transmissibility in the chaotic band is weakly dependent on λ, therefore the resonances can be suppressed with less attached mass.

V. CONCLUSION

We have studied the dispersion properties and bifurcation behaviors of NAMMs based on the HAM approach and numerical method. The local bifurcation mechanism in NAMMs, which is different from conventional local resonance, was found. It was demonstrated that the chaotic band in NAMMs is induced by the local period-doubling bifurcations of multiple cells. Bifurcations cause the disappearance of the multimodal resonances in the OB band and the generation of energy dispersion and mode interaction phenomena instead, which significantly expand the bandwidth for wave suppression. The saddle-node bifurcation makes the system state jump to the chaotic branch, along which, although the periodic solutions found by continuation approach are stable in a small interval, the responses still are chaotic. Furthermore, the nonlinear modes in the acoustic branch have bounded amplitudes even for the system without damping, which also benefits low-frequency wave suppression.

The amplitude-dependent nonlinear band gaps enable NAMMs to manipulate waves externally in the broadband. General rules of the parameters used to neatly tune the band gaps are studied: Stronger nonlinearity (which increases the amplitude A_0 or the nonlinear stiffness coefficient β_2) presents a broader nonlinear band gap and causes a larger transmission loss, while obtaining a broader band gap with less attached mass and gaining low frequency and broadbands are achievable simultaneously (but not contradictory) for nonlinear acoustic metamaterial. Moreover, only four cells are needed to generate a stable stop band and a chaotic band that suppresses the resonances; the average transmissibility in the chaotic band is weakly dependent on the mass ratio.

ACKNOWLEDGMENT

This research was funded by the National Natural Science Foundation of China (Projects No. 51405502 and No. 51275519).

APPENDIX: THEORETICAL METHOD FOR CALCULATING DISPERSION RELATIONS

For linear metamaterial $\beta_2 = 0$, Eq. (1) is transformed into a linear eigenvalue problem, which results in a linear dispersion equation

$$\omega^4 - (\alpha^2 + \beta_1 + \lambda\beta_1)\omega^2 + \alpha^2\beta_1 = 0. \tag{A1}$$

The locally resonant elements can generate the stop bands of elastic waves. This equation also indicates that the dispersion properties of linear metamaterials are relevant to the structure parameters only, but are independent of the amplitudes. The motion differential equation for the linear monatomic chain is $\ddot{u} + \alpha^2 u = 0$ and the eigenfrequency solution is $\omega_c = \alpha$. Therefore, for a finite linear monatomic chain, the normalized highest frequency of the passband is $\Omega_{\max} = \omega_{c,\max}/\omega_s = 2$.

Because multiscale techniques and perturbation methods based on linearized solutions in (A1) are proper for weak nonlinear periodic structures, this paper adopts the HAM proposed by Liao [43] to calculate the dispersion relationships. This method is compatible with strongly nonlinear systems. In the HAM, the zeroth-order deformation equations are

$$\begin{aligned}(1-q)\mathcal{L}_u[U - u_0(\tau)] &= qh_1H_1(\tau)\mathcal{N}_u[U,Y,\Lambda],\\ (1-q)\mathcal{L}_y[Y - y_0(\tau)] &= qh_2H_2(\tau)\mathcal{N}_y[U,Y,\Lambda],\end{aligned} \tag{A2}$$

where $q \in (0,1]$; $u_0(\tau)$ and $y_0(\tau)$ are initially guessed solutions of unknown parameters $u(\tau)$ and $y(\tau)$, respectively; h_i and $H_i(\tau)$ are auxiliary parameters and functions that can adjust the convergence region and velocity of the homotopy series solutions; and $\mathcal{L}(\cdot)$ and $\mathcal{N}(\cdot)$ are linear and nonlinear operators, respectively, as defined in Eq. (A3). The subscripts u and y represent the corresponding displacements

$$\begin{aligned}\mathcal{L}_u(f) &= \omega_0^2\left(\frac{d^2f}{d\tau^2} + f\right), \quad \mathcal{L}_y(f) = \omega_0^2\frac{d^2f}{d\tau^2},\\ \mathcal{N}_u[U,Y,\Lambda(q)] &= \Lambda^2(q)\frac{\partial^2U(\tau,q)}{\partial\tau^2}\\ &\quad + \alpha^2U(\tau,q) - \lambda\beta_1(Y-U) - \lambda\beta_2(Y-U)^3,\\ \mathcal{N}_y[U,Y,\Lambda(q)] &= \Lambda^2(q)\frac{\partial^2Y(\tau,q)}{\partial\tau^2}\\ &\quad + \beta_1(Y-U) + \beta_2(Y-U)^3.\end{aligned} \tag{A3}$$

The properties of the linear operators are

$$\mathcal{L}_u(c_1\sin\tau + c_2\cos\tau) = 0, \quad \mathcal{L}_y(c_3\tau + c_4) = 0. \tag{A4}$$

The initial guesses are

$$u_0(\tau) = A_0\sin\tau, \quad y_0(\tau) = B_0\sin\tau, \quad B_0 = \frac{\alpha^2 - \omega_0^2}{\lambda\omega_0^2}A_0, \tag{A5}$$

where A_0 is also the parameter of interest to control the elastic waves in the nonlinear metamaterials. Furthermore, the high-order deformation equations are

$$\begin{aligned}\mathcal{L}_u[u_m(\tau) - \chi_m u_{m-1}(\tau)] &= h_1H_1(\tau)R_m^u[U,Y,\Lambda],\\ \mathcal{L}_y[y_m(\tau) - \chi_m y_{m-1}(\tau)] &= h_2H_2(\tau)R_m^y[U,Y,\Lambda],\end{aligned} \tag{A6}$$

where

$$\chi_m = \begin{cases}0, & m = 1\\ 1, & m > 1\end{cases}$$

and

$$R_m^{u(y)}[U,Y,\Lambda] = \frac{1}{(m-1)!}\frac{\partial^{m-1}N_{u(y)}}{\partial q^{m-1}}\bigg|q = 0 \tag{A7}$$

with

$$\begin{aligned}R_m^u[U,Y,\Lambda] &= \frac{1}{(m-1)!}\frac{\partial^{m-1}\mathcal{N}_u}{\partial q^{m-1}}\bigg|q = 0\\ &= \sum_{j=0}^{m-1}u''_{m-1-j}(\tau)\left(\sum_{i=0}^{j}\omega_i\omega_{j-i}\right) + \alpha^2u_{m-1}(\tau)\\ &\quad - \lambda\beta_1[y_{m-1}(\tau) - u_{m-1}(\tau)]\\ &\quad - \lambda\beta_2\sum_{j=0}^{m-1}\sum_{i=0}^{j}[y_{m-1-j}(\tau) - u_{m-1-j}(\tau)][y_i(\tau)\\ &\quad - u_i(\tau)][y_{j-i}(\tau) - u_{j-i}(\tau)],\end{aligned}$$

$$R_m^y[U,Y,\Lambda] = \frac{1}{(m-1)!}\frac{\partial^{m-1}\mathcal{N}_y}{\partial q^{m-1}}\bigg|q=0$$
$$= \sum_{j=0}^{m-1} y''_{m-1-j}(\tau)\left(\sum_{i=0}^{j}\omega_i\omega_{j-i}\right)$$
$$+ \beta_1[y_{m-1}(\tau) - u_{m-1}(\tau)]$$
$$+ \beta_2\sum_{j=0}^{m-1}\sum_{i=0}^{j}[y_{m-1-j}(\tau) - u_{m-1-j}(\tau)][y_i(\tau)$$
$$- u_i(\tau)][y_{j-i}(\tau) - u_{j-i}(\tau)].$$

The subscript m denotes the mth-order variable. The solutions then can be approximated by the former Nth order at $q = 1$,

$$u(\tau) \approx \sum_{m=0}^{N} u_m(\tau), \quad y(\tau) \approx \sum_{m=0}^{N} y_m(\tau), \quad \omega \approx \sum_{m=0}^{N}\omega_m. \quad \text{(A8)}$$

To determine the coefficients c_i in (A4), let us define the initial boundaries of the high-order series as

$$u_m(0) = u'_m(0) = 0, \quad m \geqslant 1.$$

With the base functions $\{\sin\tau, \sin 3\tau, \ldots, \sin(2m-1)\tau\}$, $R_m^u(\tau)$ and $R_m^y(\tau)$ can be expressed as

$$R_m^u(\tau) = a_{m,1}\sin\tau + \sum_{j=2}^{M} a_{m,j}\sin(2j-1)\tau,$$
$$R_m^y(\tau) = \sum_{j=1}^{M} b_{m,j}\sin(2j-1)\tau. \quad \text{(A9)}$$

The parameters $a_{m,j}$ and $b_{m,j}$ are relevant to the unknown frequencies ω_{j-1}. Because the expressions in (A9) already include all base functions and the solutions of the linear operators also contain the base functions, the auxiliary functions can be defined as constants $H_i(\tau) = 1$. Furthermore, to avoid the secular terms $\tau\sin\tau$ and $\tau\cos\tau$ in $u_m(\tau)$,$a_{m,j} = 0$ must be in (A9). This formula leads to the solution of ω_{j-1}. In addition, to avoid the secular terms τ^m in $y_m(\tau)$, $c_3 = c_4 = 0$ must be in (A4). The boundary condition $u_m(0) = 0$ leads to $c_2 = 0$. Moreover, the coefficient c_1 can be obtained with $u'_m(0) = 0$.

However, for arbitrary convergence-control parameters h_1 and h_2, the Taylor series in Eq. (A8) expanded in the zero domain converges slowly or even cannot converge at $q = 1$, which means that the two parameters should be chosen properly. The homotopy Padé approximant [43] provides the convergent solutions in a sufficiently large region. The $[m,n]$-order Padé approximant is expressed as

$$\Lambda_{m,n}(q) = \left(\sum_{k=0}^{m} P_k q^k\right)\Big/\left(1 + \sum_{k=1}^{n} P_{m+1+k}q^k\right), \quad \text{(A10)}$$

where P_k depends on ω_m. Setting $q = 1$ in Eq. (A10) will obtain a rapidly convergent solution; therefore, the $[m,n]$ Padé approximant of the frequency is $\omega^{(m,n)} = \Lambda_{m,n}(1)$. Generally, $\omega^{(2,2)}$ and $\omega^{(3,3)}$ are sufficiently accurate for the nonlinear metamaterial model. For example,

$$\omega^{(2,\,2)} = \omega_0 + \frac{\omega_1^2(\omega_4-\omega_3) + \omega_2^3 + \omega_1\omega_2(\omega_2 - 2\omega_3)}{\omega_2^2 + \omega_3^2 + \omega_1(\omega_4-\omega_3) - \omega_2(\omega_4+\omega_3)}. \quad \text{(A11)}$$

The homotopy Padé technique is a combination of the conventional Padé technique with the homotopy analysis method. If the convergence-control parameters (especially the h_1 and h_2) and the order of the Padé approximant are chosen properly, the approach will converge to the exact solutions even under strong nonlinearities.

[1] N. I. Zheludev, Science **328**, 582 (2010).
[2] Z. Liu, X. Zhang, Y. Mao, Y. Y. Zhu, Z. Yang, C. T. Chan, and P. Sheng, Science **289**, 1734 (2000).
[3] S. A. Cummer, J. Christensen, and A. Alù, Nat. Rev. Mater. **1**, 16001 (2016).
[4] G. Wang, X. Wen, J. Wen, L. Shao, and Y. Liu, Phys. Rev. Lett. **93**, 154302 (2004).
[5] C. Shen, Y. Xie, N. Sui, W. Wang, S. A. Cummer, and Y. Jing, Phys. Rev. Lett. **115**, 254301 (2015).
[6] Z. Yang, J. Mei, M. Yang, N. H. Chan, and P. Sheng, Phys. Rev. Lett. **101**, 204301 (2008).
[7] M. Rupin, F. Lemoult, G. Lerosey, and P. Roux, Phys. Rev. Lett. **112**, 234301 (2014).
[8] P. Wang, F. Casadei, S. Shan, J. C. Weaver, and K. Bertoldi, Phys. Rev. Lett. **113**, 014301 (2014).
[9] L. Cai, X. Han, and X. Wen, Phys. Rev. B **74**, 153101 (2006).
[10] Y. Xiao, J. Wen, and X. Wen, New J. Phys. **14**, 033042 (2012).
[11] G. Ma, Y. Min, S. Xiao, Z. Yang, and P. Sheng, Nat. Mater. **13**, 873 (2014).
[12] T. Brunet, J. Leng, and M.-M. Olivier, Science **342**, 323 (2013).
[13] M. I. Hussein, M. J. Leamy, and M. Ruzzene, Appl. Mech. Rev. **66**, 040802 (2014).
[14] B. Liang, B. Yuan, and J. C. Cheng, Phys. Rev. Lett. **103**, 104301 (2009).
[15] R. Ganesh and S. Gonella, Phys. Rev. Lett. **114**, 054302 (2015).
[16] A. F. Vakakis, Acta Mech. **95**, 197 (1992).
[17] N. Boechler, G. Theocharis, and C. Daraio, Nat. Mater. **10**, 665 (2011).
[18] F. Li, P. Anzel, J. Yang, P. G. Kevrekidis, and C. Daraio, Nat. Commun. **5**, 5311 (2014).
[19] C. Daraio, V. F. Nesterenko, E. Herbold, and S. Jin, Phys. Rev. E **73**, 026610 (2006).
[20] K. L. Manktelow, M. J. Leamy, and M. Ruzzene, Nonlinear Dyn. **63**, 193 (2011).
[21] M. Scalora, M. J. Bloemer, A. S. Manka, J. P. Dowling, C. M. Bowden, R. Viswanathan, and J. W. Haus, Phys. Rev. A **56**, 3166 (1997).
[22] T. Meurer, J. Qu, and L. Jacobs, Int. J. Solids Struct. **39**, 5585 (2002).

[23] N. Boechler, G. Theocharis, S. Job, P. G. Kevrekidis, M. A. Porter, and C. Daraio, Phys. Rev. Lett. **104**, 244302 (2010).
[24] E. Kim, F. Li, C. Chong, G. Theocharis, J. Yang, and P. G. Kevrekidis, Phys. Rev. Lett. **114**, 118002 (2015).
[25] S. Y. Wang and V. F. Nesterenko, Phys. Rev. E **91**, 062211 (2015).
[26] H. Pichard, A. Duclos, J.-P. Groby, V. Tournat, L. Zheng, and V. E. Gusev, Phys. Rev. E **93**, 023008 (2016).
[27] X. Fang, C. H. Zhang, X. Chen, Y. S. Wang, and Y. Y. Tan, Acta Mech. **226**, 1657 (2015).
[28] V. F. Nesterenko, *Dynamics of Heterogeneous Materials* (Springer, New York, 2001).
[29] J. Lydon, G. Theocharis, and C. Daraio, Phys. Rev. E **91**, 023208 (2015).
[30] R. K. Narisetti, M. Ruzzene, and M. J. Leamy, J. Vib. Acoust. **133**, 061020 (2011).
[31] R. K. Narisetti, M. Ruzzene, and M. J. Leamy, Wave Motion **49**, 394 (2012).
[32] K. Manktelow, M. J. Leamy, and M. Ruzzene, J. Mech. Phys. Solids **61**, 2433 (2013).
[33] B. Yousefzadeh and A. S. Phani, J. Sound. Vib. **354**, 180 (2015).
[34] B. P. Bernard, M. J. Mazzoleni, N. Garraud, D. P. Arnold, and B. P. Mann, J. Appl. Phys. **116**, 084904 (2014).
[35] E. B. Herbold, J. Kim, V. F. Nesterenko, S. Y. Wang, and C. Daraio, Acta Mech. **205**, 85 (2009).
[36] Y. Xu and V. F. Nesterenko, Philos. Trans. R. Soc. London A **372**, 20130186 (2014).
[37] C. M. Donahue, P. W. J. Anzel, L. Bonanomi, T. A. Keller, and C. Daraio, Appl. Phys. Lett. **104**, 014103 (2014).
[38] D. Midtvedt, A. Isacsson, and A. Croy, Nat. Commun. **5**, 4838 (2014).
[39] R. M. Rosenberg, Adv. Appl. Mech. **9**, 155 (1966).
[40] S. W. Shaw and C. Pierre, J. Sound. Vib. **150**, 170 (1991).
[41] S. W. Shaw and C. Pierre, in *Nonlinear Vibrations, Proceedings of the Winter Annual Meeting of the ASME, Anaheim, 1992*, edited by R. A. Ibrahim, N. S. Namachchivaya, and A. K. Bajaj (ASME, New York, 1992).
[42] G. Kerschen, M. Peeters, J. C. Golinval, and A. F. Vakakis, Mech. Syst. Signal Process. **23**, 170 (2009).
[43] S. J. Liao, *Homotopy Analysis Method in Nonlinear Differential Equations* (Springer, New York, 2011).
[44] C. Hoogeboom *et al.*, Europhys. Lett. **101**, 44003 (2013).
[45] E. J. Doedel and B. E. Oldeman AUTO-07P, Continuation and bifurcation software for ordinary differential equations, 2012, available at http://indy.cs.concordia.ca/auto